Published in final edited form as:

Xie, W. J., Cha, S., Ohto, T., Mizukami, W., Mao, Y., Wagner, M., et al. (2018). Large Hydrogen-Bond Mismatch between TMAO and Urea Promotes Their Hydrophobic Association. Chem, 4(11), 2615-2627. doi:10.1016/j.chempr.2018.08.020.

Link to formal publication: 10.1016/j.chempr.2018.08.020

Supplemental Information

Large Hydrogen-Bond Mismatch between TMAO and Urea Promotes Their Hydrophobic Association

Wen JunXie, Seoncheol Cha, Tatsuhiko Ohto, Wataru Mizukami, Yuezhi Mao, Manfred Wagner, Mischa Bonn, Johannes Hunger, Yuki Nagata

Supplemental Information

Large Hydrogen-Bond Mismatch between TMAO and Urea Promotes Their Hydrophobic Association

Wen Jun Xie, Seoncheol Cha, Tatsuhiko Ohto, Wataru Mizukami, Yuezhi Mao, Manfred Wagner, Mischa Bonn, Johannes Hunger, and Yuki Nagata

Table of Contents

1. Supplemental Data of MD Simulations

a. Choice of reaction coordinate

In the main text, we used the O_{TMAO}-C_{UREA} distance as reaction coordinate to compute the PMF. Here, we computed the PMF data by using the N_{TMAO}-C_{UREA} distance as a reaction coordinate. Figure S1(a) shows that the PMF as a function of N_{TMAO}-C_{UREA} distance has only one minimum, unlike the PMF data as a function of O_{TMAO}-C_{UREA} distance. This reaction coordinate fails to distinguish between the hydrophobic and hydrophilic interactions.

In fact, for the N_{TMAO}-C_{UREA} distance of 4.60 Å, we found both H-bonded TMAO-urea conformations (Figure S1(b)) and hydrophobically associated TMAO-urea conformations (Figure S1(c)). As such, the O_{TMAO}-C_{UREA} distance is a good reaction coordinate for distinguishing the H-bonded conformation from the hydrophobic association conformation.

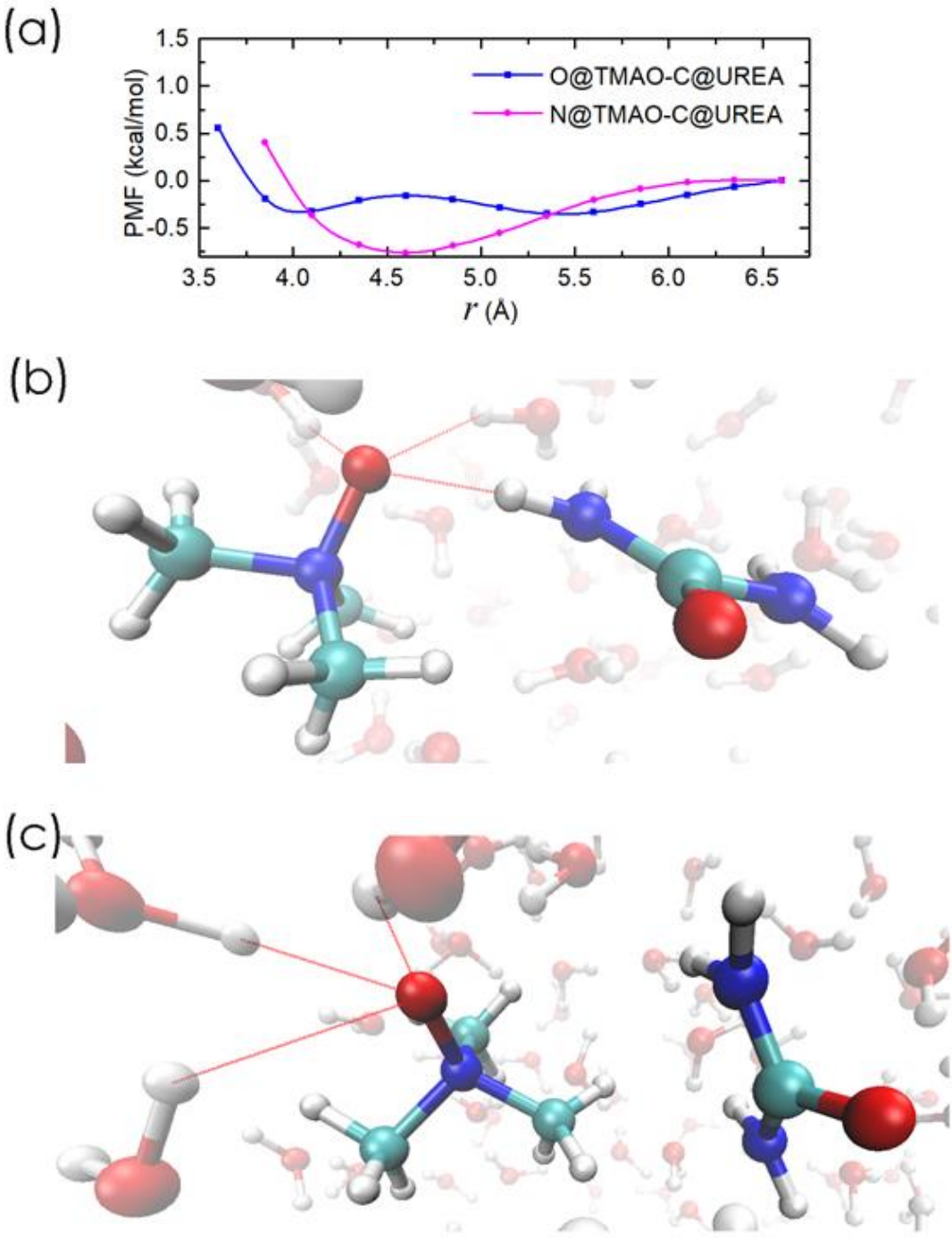

Figure S1: Comparison of PMF in the Kast/OPLS FFMD simulations with different reaction coordinates. (a) TMAO-urea PMF. (b) the H-bonded conformation and (c) the hydrophobic association conformation both exhibit a minimum in the PMF at $r(N_{TMAO}\text{-}C_{UREA})$ = 4.60 Å.

b. Effect of temperature on the TMAO-urea PMF

In the MD simulations for calculating the PMF, we used relatively high temperature (380 K) to accelerate the sampling in the whole phase-space. To examine the effects of the elevated temperature on the PMF, we also carried out the FFMD simulation with the Netz/KB model at 300 K and compared it with the PMF at 380 K. The simulation conditions such as cell size and ensemble were the same as the FFMD simulation at 380 K. The data is displayed in Figure S2. For both temperatures, we can see one minimum around r = 5.8 Å. Furthermore, the difference in the PMFs at 300 K and 380 K is at most 0.2 kcal/mol. Thus, the elevated temperature at 380 K does not significantly affect the trends in the reported PMFs.

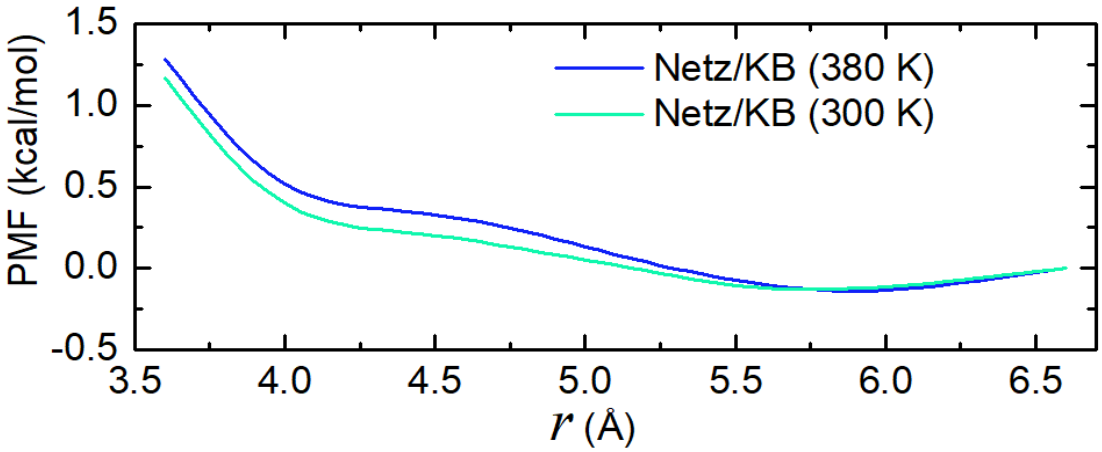

Figure S2. Effect of temperature on the TMAO-urea PMF using the Netz/KB models.

c. Effect of simulation cell size on the TMAO-urea PMF

To examine the effect of the simulation cell size on the PMF, we calculated the PMF using the large simulation cell in FFMD simulation. This simulation cell contained one TMAO molecule, one urea molecule and 610 water molecules with a cell size of $(26.40\ \text{Å})^3$, resulting in a density of 1.00 g/cm^3. The separation distance r ranges from 3.60 Å to 10.60 Å with an interval of 0.25 Å. The other simulation conditions such as target temperature and ensembles were the same as the FFMD simulation with a simulation cell size of $(17.075\ \text{Å})^3$.

The comparison between the constraint force and PMF in the large simulation cell ($(26.40\ \text{Å})^3$) and the small simulation cell ($(17.075\ \text{Å})^3$) are shown in Figure S3. The values of intermolecular constraint force for r < 6.60 Å coincide quite well between FFMD simulations with the large simulation cells and with the small simulation cells. This demonstrates that the cell size of $(17.075\ \text{Å})^3$ suffices to compute the PMF of TMAO and urea.

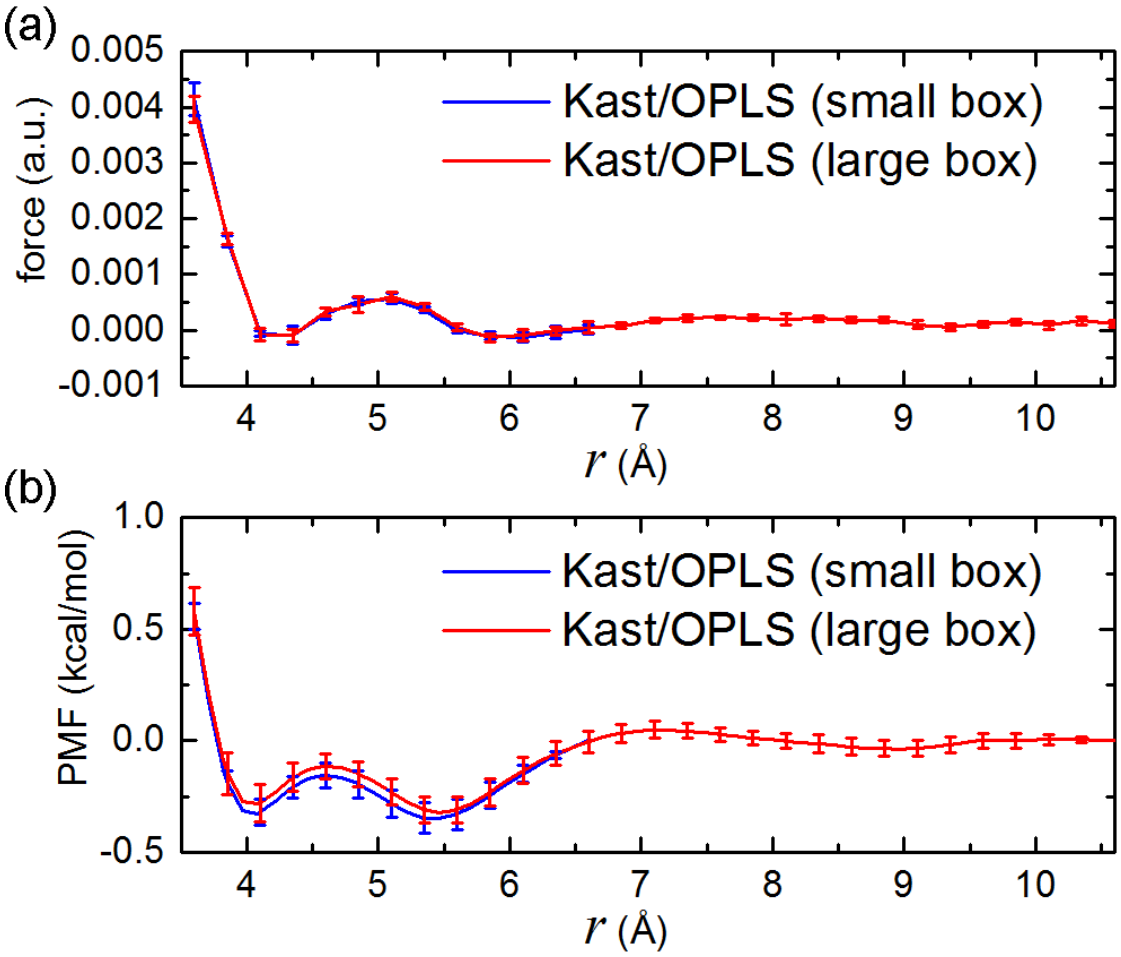

Figure S3. Comparison of constraint force and PMF in the FFMD simulation with different simulation cell sizes. (a) Constraint force. (b) PMF. The simulation boxes with cell sizes of (26.40 Å)^3 and (17.075 Å)^3 are respectively denoted as large box and small box in the figure legend.

d. Hydrophobic interaction between TMAO and urea

The variation of LJ radius should affect the hydrophobic interactions of TMAO. To measure how the PMFs are affected by this LJ radius, we varied the radius parameter of the LJ potential for the H_{TMAO} and C_{TMAO} atoms. The radii were obtained by combining the LJ radii of the Kast TMAO model (σ_{Kast})[41] and the Netz TMAO model (σ_{Netz})[39]. In the Kast and Netz TMAO models, the LJ radii of the C_{TMAO} and H_{TMAO} atoms are different, while the O_{TMAO} and N_{TMAO} atoms have the same LJ radii. The well depths of the LJ potentials are the same for all the atoms in the two models. We summarized the LJ radii for TMAO models in Table S1.

The PMFs simulated with various LJ radii are shown in Figure S4. The larger LJ radius of the TMAO methyl groups shifts the location of the PMF minimum at r = 5.4 Å to longer r. This indicates that the PMF minimum at r = 5.4 Å likely originates from hydrophobic interaction

between TMAO and urea. Contrarily, the variation of the LJ radius of the methyl group does not change the relative depths of the PMF minima at r = 4.1 Å and r = ~5.4 Å, suggesting that the PMF minima at r = 4.1 Å are not due to hydrophobic interaction.

Table S1. The LJ radii for TMAO models used for Figure S4

Combination of vdW radii	**vdW radius of C_{TMAO} (Å)**	**vdW radius of H_{TMAO} (Å)**
σ_{Kast} [41]	3.041	1.775
$0.75\sigma_{Kast} + 0.25\sigma_{Netz}$	3.18075	1.8565
$0.50\sigma_{Kast} + 0.50\sigma_{Netz}$	3.3205	1.938
$0.25\sigma_{Kast} + 0.75\sigma_{Netz}$	3.46025	2.0195
σ_{Netz} [39]	3.600	2.101

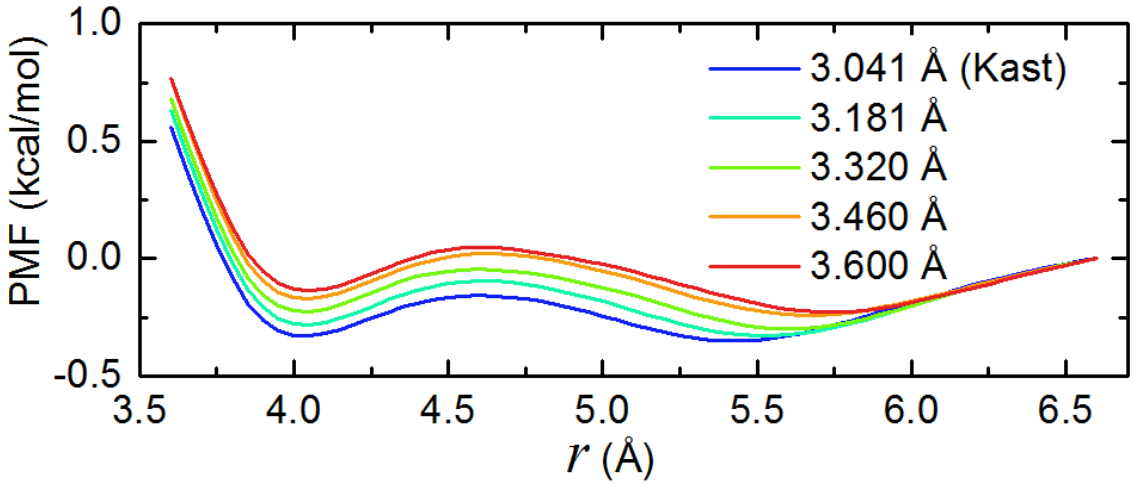

Figure S4. PMFs of the FFMD simulation when varying the LJ radius of C_{TMAO} and H_{TMAO} atoms.

e. PMFs using the Netz TMAO model, the Shea TMAO model, and the KB urea model

It has been shown that both the Kast TMAO model and OPLS urea models are not perfect; the poor reproduction of the macroscopic observables such as the concentration-dependent density of aqueous TMAO solutions and the solution activity coefficients with the Kast TMAO model was pointed out in previous studies[39, 40], motivating improvement of the force field models. New force field models including the Shea[40] and Netz[39] TMAO models were developed recently, in addition to several other models.[S1, S2] The Shea TMAO model could reproduce the number of hydration water and the Netz TMAO model could reproduce the H-bond dynamics of water.[32] The KB urea

model can reproduce solution thermodynamics of urea-water system and improves the performance of urea self-aggregation.[15] The combinations of the KB urea and the Kast, Netz, Shea for TMAO were also used to study the solvation of amino acids.[4]

Based on these findings, we also calculated the TMAO-urea PMF using recently developed force field models (the Shea TMAO model[40] and the Netz TMAO model,[39] together with the KB urea model[15]). The PMFs using the OPLS urea model and the KB urea model are shown in Figure S5(a) and (b), respectively. At r = ~4.1 Å, the values of the PMFs follow the order of Netz model > Shea model > Kast model, independent of the urea model. The speed of the H-bond dynamics also follows the order of Netz model < Shea model < Kast model (Figure 4 in Ref. 32). Consistent with our conclusion in the main text, we can correlate the order of the H-bond dynamics with the PMF. The Netz TMAO model shows the slowest H-bond dynamics, which has the largest deviation with urea H-bond dynamics. Therefore, the PMF at r = ~4.1 Å using the Netz TMAO model is the highest.

When we used the KB urea model instead of the OPLS model, the PMFs increase at r = ~4.1 Å. We have seen that the KB urea model shows a faster H-bond dynamics than the OPLS urea (Figure S7). The deviation between the H-bond dynamics of TMAO and urea would increase when using the KB urea. Thus, the PMF using the KB urea is higher than that using the OPLS urea.

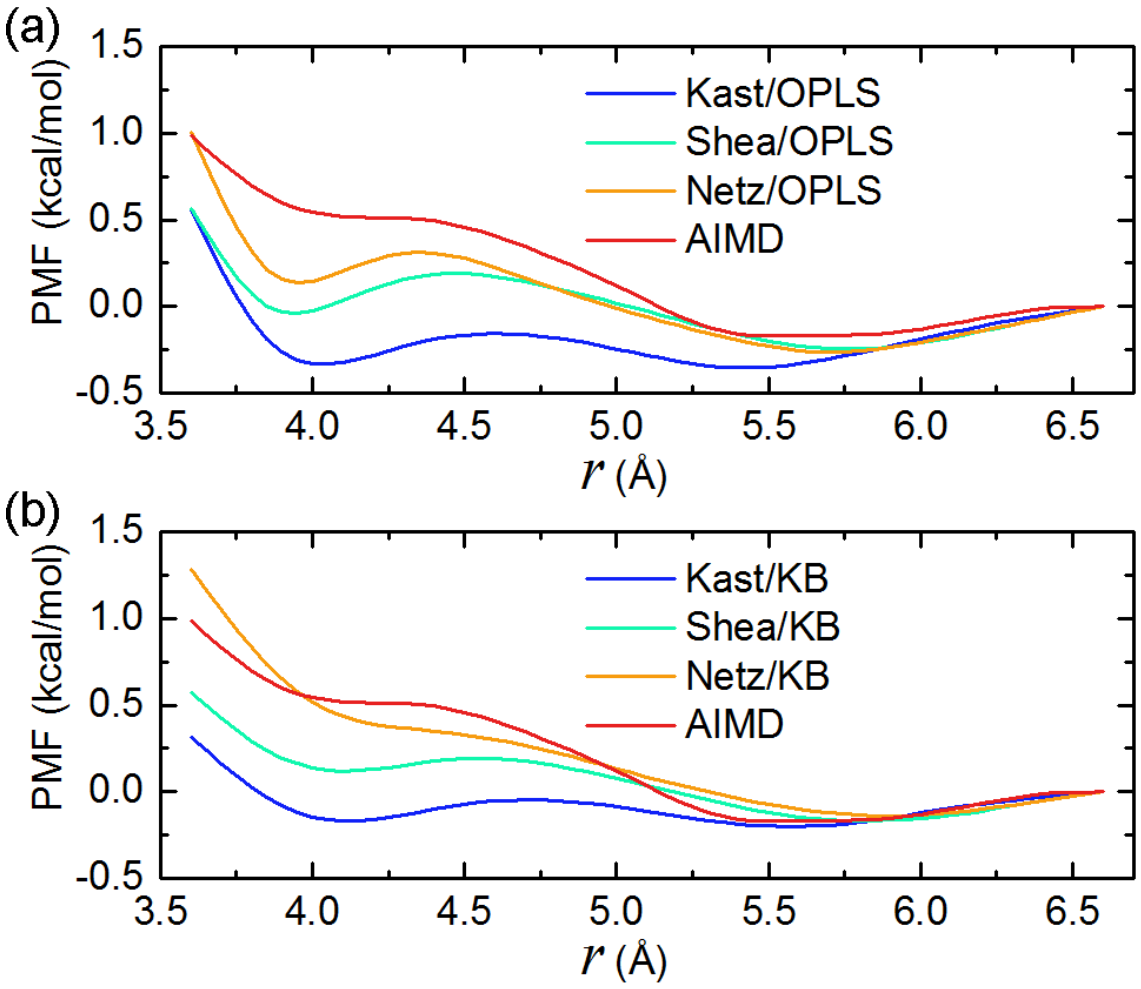

Figure S5. TMAO-urea PMFs using different TMAO models and urea models. The PMF obtained from AIMD (BLYP) simulation is also shown for comparison.

f. H-bond dynamics

The H-bond dynamics were computed as the H-bond time correlation function;[42]

$$P_{\mathrm{HB}}(t) = \frac{\langle h(0)h(t)\rangle}{\langle h(0)\rangle} \qquad \text{(Equation S1)}$$

where $h(t)$ is unity when the H-bond is formed, 0 otherwise. The same H-bond definition as the above calculation was used for evaluating the H-bond dynamics.

Figure 3 in the main text shows the more pronounced difference in the O_{TMAO}…H_W and H_{UREA}…O_W H-bond dynamics in the AIMD simulation as compared to the FFMD simulation. Here, we plotted the variation of the H-bond dynamics when we changed the charges of TMAO (See Table S6) and of urea (See Table S7). We can see that the increase in the absolute value

of the O_{TMAO} charge slows down the H-bond dynamics of TMAO-water, and a decrease in the H_{UREA} charge accelerates the H-bond dynamics of urea-water (Figure S6).

Further data are obtained by using the KB urea model.[15] Figure S7 depicts the comparison of the H-bond dynamics of the OPLS urea model and the KB urea model. The H-bond dynamics of the KB urea is faster than the OPLS urea. This result that the KB urea model shows faster H-bond dynamics than the OPLS urea model is consistent with KB model having weaker H-bond with water. [15]

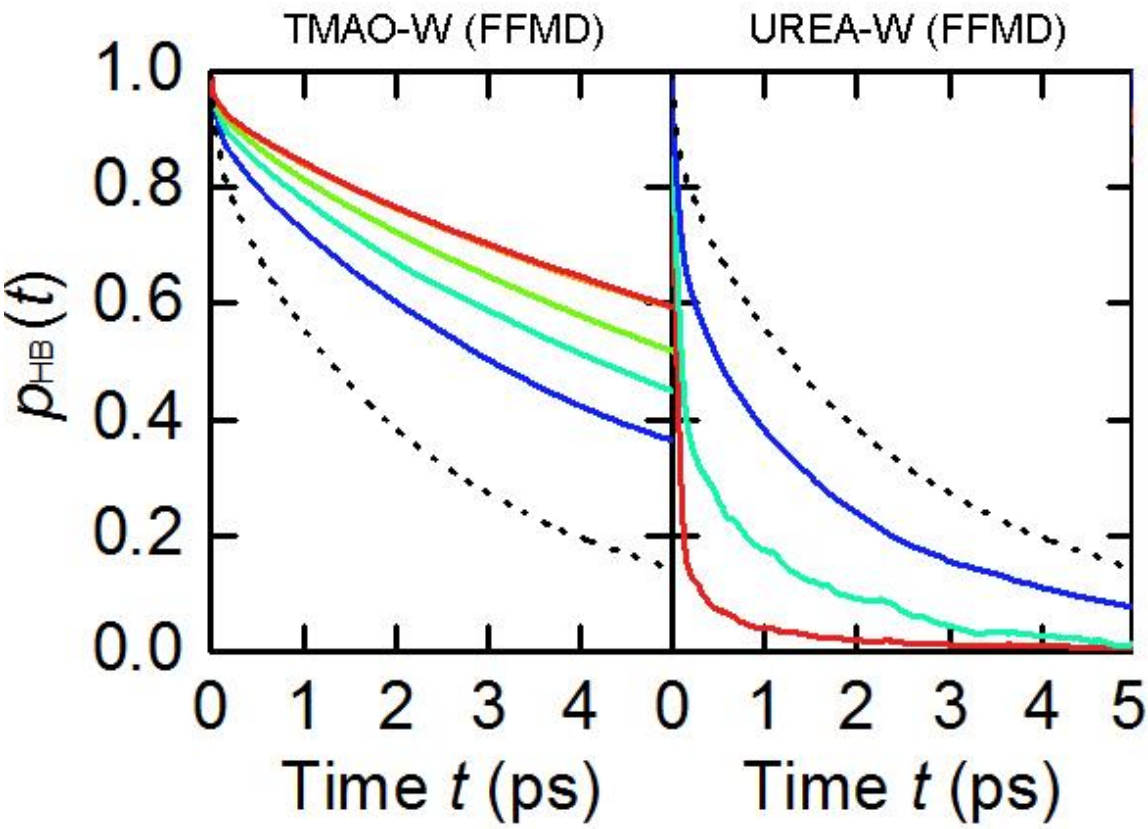

Figure S6. Simulated H-bond dynamics. (a) O_{TMAO}…H_W H-bond dynamics and (b) H_{UREA}…O_W H-bond dynamics simulated in the FFMD. The color codes of the solid lines are the same as Figure 2A and 2B, respectively, while the dotted black line represents the O_W…H_W H-bond dynamics.

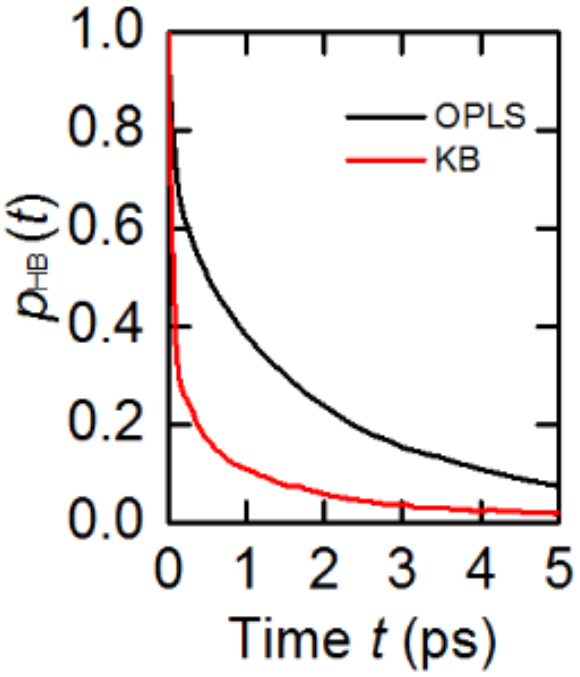

Figure S7. Comparison of H-bond dynamics of the OPLS urea model and the KB urea model.

g. Conformational energy of H-bonded dimer of TMAO-urea, TMAO-water from force field

We calculated the conformational energy of TMAO-urea H-bonded dimer and TMAO-water H-bonded dimer from force fields. The TMAO-urea H-bonded dimer configurations were extracted from the FFMD at the TMAO-urea separation of 4.10 Å. These are summarized in Table S2. This shows that the Kast TMAO model combined with the OPLS urea model provides a stronger TMAO-urea H-bond than TMAO-water H-bond, consistent with the report from Paul and Patey.[9] In contrast, the relative stabilities of the two H-bonds are reversed when using the Netz TMAO model combined with the KB urea model.

Table S2. H-bond energy (in kcal/mol) of TMAO-urea H-bond and TMAO-water H-bond. The errors represent the 95% confidence intervals.

	TMAO-urea	**TMAO-water**
Kast/OPLS	-8.30±0.01	-7.10±0.01
Netz/KB	-8.87±0.01	-10.50±0.01

h. Convergence check of simulation data

We evaluated the error of the simulated PMF data. Figure S8 displays the PMF data with the error bars (90 % confidence intervals). This shows that the errors are smaller than the PMF energy difference in the H-bonded and hydrophobically interacted TMAO-urea conformation.

Furthermore, to quantify whether the 8 × 20 ps AIMD trajectories are adequate to converge the simulated PMF, we used the first 20 ps trajectories of each of the eight 1 ns simulation data obtained in the FFMD simulation with the Netz/KB model. The data are shown in Figure S9. The PMF with the 8 × 20 ps FFMD trajectories is quite similar to the PMF obtained from the 8 × 1 ns FFMD trajectories, suggesting that the 8 × 20 ps simulation data is enough to calculate the TMAO-urea PMF.

Relatively rapid convergence of the PMF data with a limited length of the trajectory likely arises from the high symmetry of the TMAO and urea molecules. Furthermore, the TMAO and urea rotates very quickly at 380 K. The rotational relaxation time for the NO vector of the Netz TMAO and the CO vector of the KB urea are 9.2 ps and 2.5 ps, respectively. As such, a total 160 ps is adequate to sample the whole phase space.

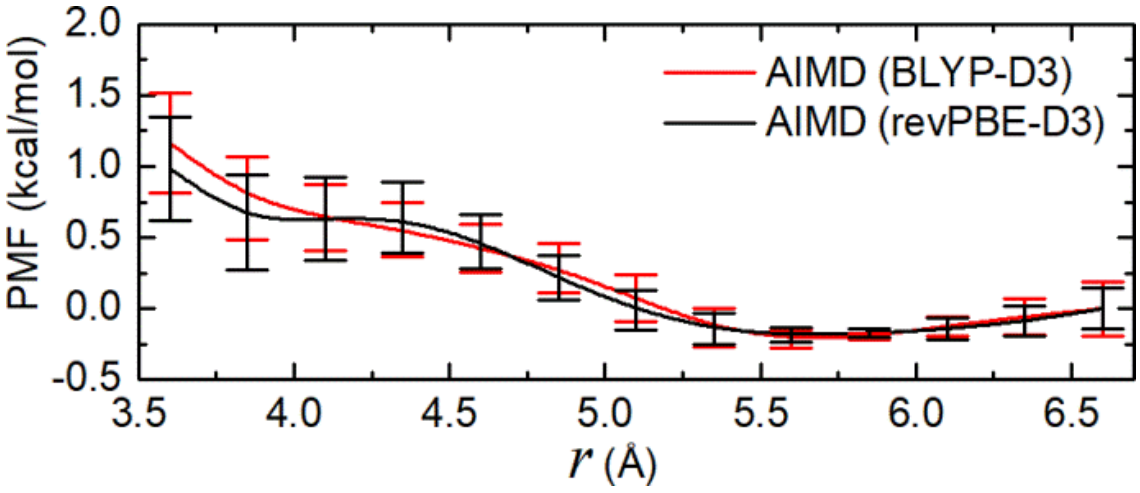

Figure S8. The PMFs obtained from AIMD and Kast/OPLS FFMD simulations. 90% confidence intervals of PMFs from AIMD simulations are plotted.

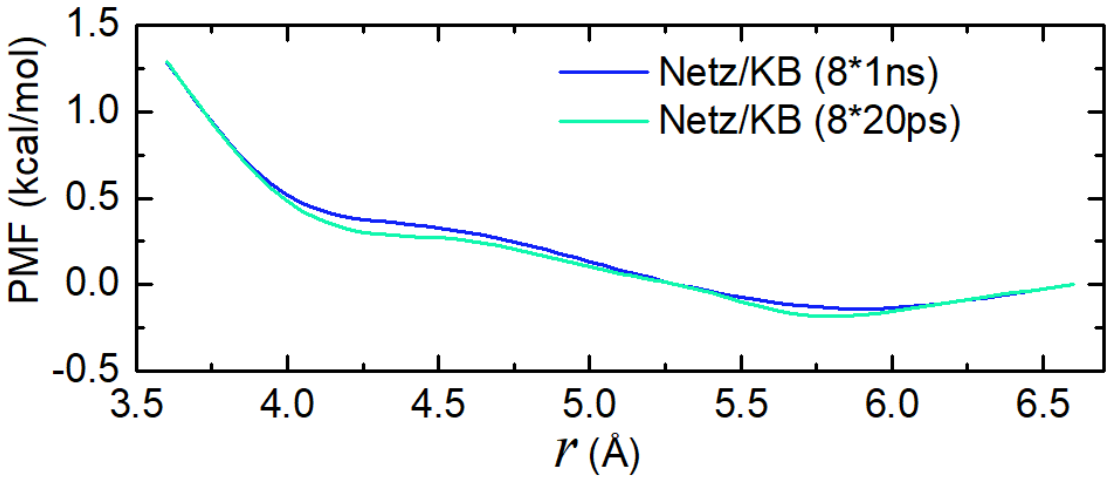

Figure S9. Comparison of PMFs using the 8 × 20 ps and 8 × 1 ns MD simulation data obtained with the Netz/KB model.

i. PMF obtained from long AIMD simulation trajectories

In the main text, we reported the TMAO-urea PMF by averaging the values over 8 independent AIMD trajectories (Figure 1). Due to the high computational cost of AIMD simulation, the simulation length for each TMAO-urea separation in each independent trajectory was 20 ps. To further confirm that the AIMD PMF data is fully converged, we compare the AIMD PMF data for 8 × 20 ps samples with that obtained from a 130 ps AIMD trajectory at the BLYP/TZV2P-D3 level of theory.

The PMF computed from the 130 ps AIMD trajectories is shown in Figure S10 (denoted as "long-time"). The PMF have a shallow minimum in 5.3 Å ≤ r ≤ 5.7 Å and is increasingly unfavorable with a short $O_{TMAO}…C_{UREA}$ separation of r < 5.3 Å. These trends are consistent with the PMF reported in the main text.

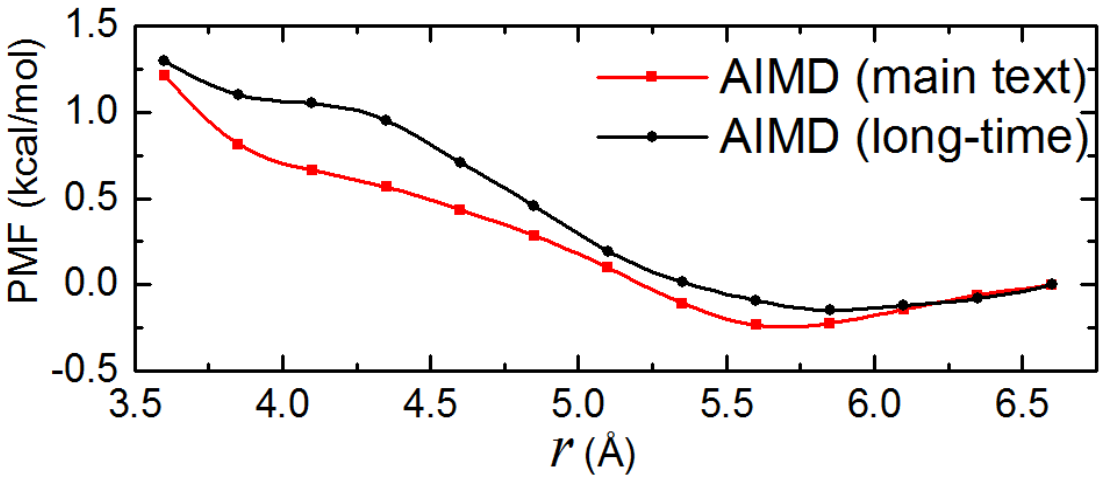

Figure S10. Comparisons of PMFs in different AIMD simulation trajectories at the BLYP/TZV2P-D3 level of theory. The PMF obtained from eight independent trajectories (8 × 20 ps) is shown in red, while the PMF using the long-time AIMD 130 ps trajectory for a single initial coordinate is shown in black.

j. Conformational energy of H-bonded dimer of TMAO-urea, TMAO-water, urea-water from DFT calculation

Based on DFT calculation, the relative strengths of TMAO-urea, TMAO-water and urea-water hydrogen bonds could also be investigated based on the dimer interaction energies between the associated species. The dimer configurations were extracted from the corresponding AIMD trajectories (for TMAO-urea, we used the AIMD trajectory where the separation between TMAO and urea was restrained to be 4.10 Å) at the BLYP-D3/TZV2P level of theory.

The single-point energy calculations were performed with the Q-Chem 5.0 software package.[S3] To examine the consistency of evaluated H-bond strengths with respect to the choice of density functional, five density functionals (BLYP-D3[36], revPBE-D3[37], revPBE0-D3[37, S4], B97M-rV[S5, S6] and ωB97X-V[S7] were employed (the first three functionals used the original "zero" damping function[38] for the D3 correction). The def2-TZVPPD basis set[S8] was utilized for these calculations. The results are summarized in Table S3. The TMAO-water H-bond is in general stronger than the TMAO-urea H-bond in terms of the dimer interaction energy, while urea binds less strongly to water than to TMAO. The same trend holds for all five functionals employed here.

Table S3. Interaction energies (in kcal/mol) for H-bonded pairs (TMAO-urea, TMAO-water and urea-water) evaluated with five density functionals and the def2-TZVPPD basis set. For each H-bonded pair, the interaction energy was averaged over 200 dimer configurations. The errors represent the 90% confidence intervals.

	TMAO-urea	**TMAO-water**	**urea-water**
BLYP-D3	-9.95±0.23	-10.68±0.21	-3.65±0.18
revPBE-D3	-9.54±0.23	-10.09±0.20	-3.31±0.18
revPBE0-D3	-10.05±0.24	-10.67±0.21	-3.66±0.18
B97M-rV	-10.02±0.23	-10.48±0.20	-3.88±0.18
***ω*B97X-V**	-10.19±0.23	-10.85±0.21	-3.77±0.18

The calculations of dimer interaction energies above were performed in vacuum. In order to take the solvent environment into account, we also calculated the interaction energies for the same set of dimer configurations with the BLYP-D3 functional and a polarizable continuum model (PCM)[S9] of water (whose dielectric constant is set to 78.39). The results are shown in Table S4. The average binding energy of each H-bonded pair is shifted using implicit solvent model compared to that in vacuum. However, the relative order of the H-bond strengths does not change. Interestingly, we found that the difference between the strengths of TMAO-water and TMAO-urea H-bonds is more pronounced compared to that in vacuum.

Table S4. Interaction energies (in kcal/mol) for H-bonded pairs (TMAO-urea, TMAO-water and urea-water) evaluated with BLYP-D3/def2-TZVPPD. Implicit solvent model (PCM water, $\varepsilon = 78.39$) was used. The error represents the 90% confidential intervals.

TMAO-urea	**TMAO-water**	**urea-water**
-5.40 ± 0.14	-8.32 ± 0.18	-2.37 ± 0.13

From both the Netz/KB force field and DFT calculation, TMAO-urea H-bond is less stable than TMAO-water H-bond. This is consistent with their similar TMAO-urea PMF profile obtained using these models.

k. Electrostatic vs. dispersion interaction energies

Figure S11 shows the computed electrostatic vs. dispersion interaction energies for the conformation of TMAO and urea with r = 3.85 Å and 5.60 Å. For the TMAO-urea conformation

with r = 3.85 Å, the electrostatic interaction governs the TMAO-urea stabilization, while the dispersion energy governs for the TMAO-urea conformation with r = 5.60 Å. As such, we conclude that TMAO-urea conformation with r ~ 3.85 Å is governed by electrostatic (H-bond) interaction, while the dispersion (hydrophobic) interaction contributes to the conformational energy for TMAO-urea with r ~ 5.60 Å than the electrostatic energy.

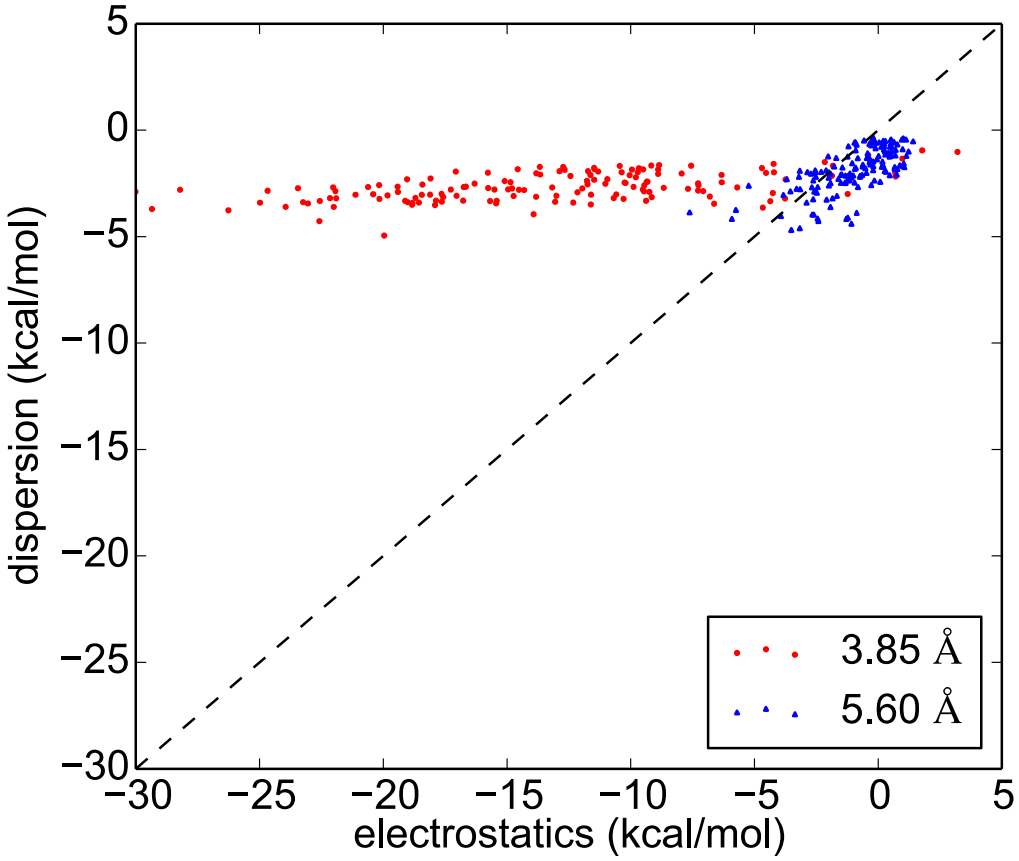

Figure S11: Scatter plots of dispersion energy (y axis) vs. electrostatic energy (x axis) obtained from ALMO-EDA calculations for configurations with r = 3.85 Å and r = 5.60 Å. Points above the black broken line (diagonal line) indicate that electrostatic interaction dominates the energy stabilization, while points below the diagonal line indicate that dispersion energy dominates.

I. H-bond number between TMAO and urea

TMAO and urea can form H-bond in which TMAO acts as H-bond acceptor and urea is H-bond donor. As mentioned in the main text, the H-bond number is defined as unity when 1.59 Å < $r_{O...H}$ < 2.27 Å,[S10] where O and H denote the oxygen and hydrogen atoms involved in the H-bond formation, respectively. The average H-bond number between TMAO and urea in AIMD

simulation was shown in Figure S12. We found directly H-bonded TMAO-urea conformation at r ≤ ~4.1 Å, which is consistent with the assignment made in the main text.

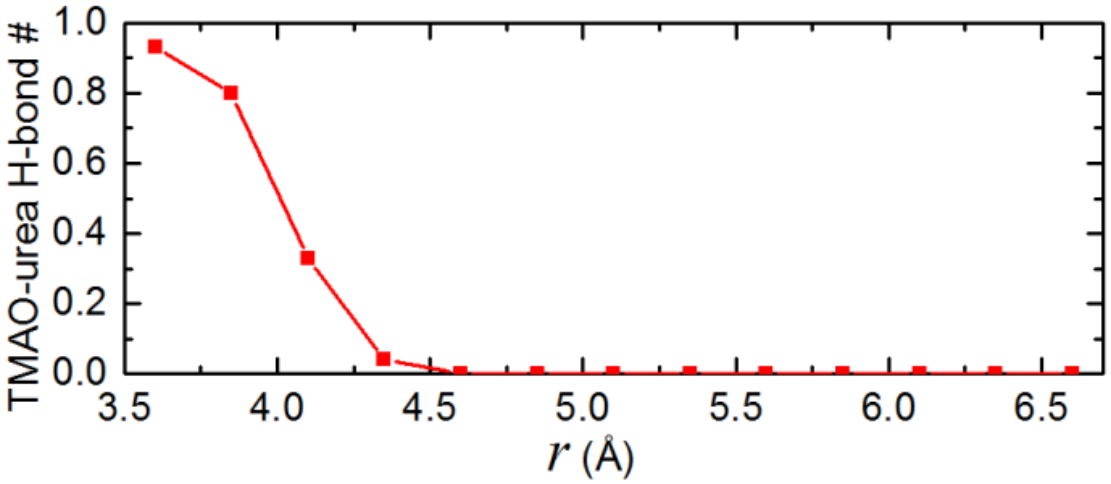

Figure S12. Average H-bond number between TMAO and urea in AIMD simulation.

2. Supplemental Data of TR-IR Experiment

As indicated in the main text of the manuscript, both HOD molecules H-bonded to water and H-bonded to TMAO contribute to the observed transient signals. Both TMAO and urea do not affect the isotropic decay at the center of the $O_W…D_W$-O_W H-bonded O-D stretching peak at 2500 cm^{-1} (see Figure S13(b)). As some of us have shown previously,[11, 32] the $O_{TMAO}…D_W$-O_W are centered at red-shifted frequencies, relative to $O_W…D_W$-O_W H-bonded O-D groups. Consistent with this earlier study, at a TMAO concentration as low as 2 M the isotropic dynamics at 2470 cm^{-1} is hardly affected by the presence of these red-shifted $O_{TMAO}…D_W$-O_W groups (see Figure S13(a)). Noteworthy, urea does not affect the isotropic decays at both frequencies, which indicates that urea does not alter the H-bonded structure of the studied solutions significantly.

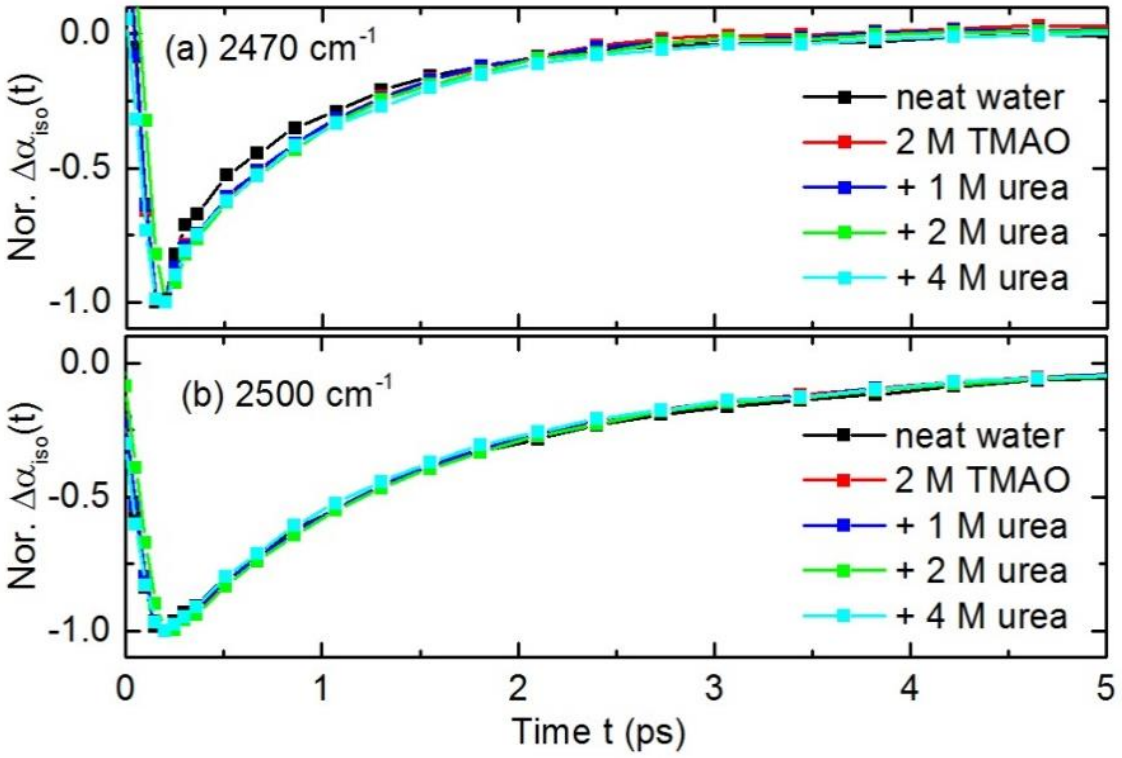

Figure S13. Normalized time-dependent transient absorption, $\Delta\alpha_{iso}(t)$ at (a) 2470 cm^{-1} and (b) 2500 cm^{-1} for aqueous solutions (5 wt% HOD in H_2O) containing different concentrations of TMAO and urea.

3. Supplemental Data of NMR Experiment

The comparison of the NMR chemical shift for TMAO, urea, and DMSO is shown in Figure S14.

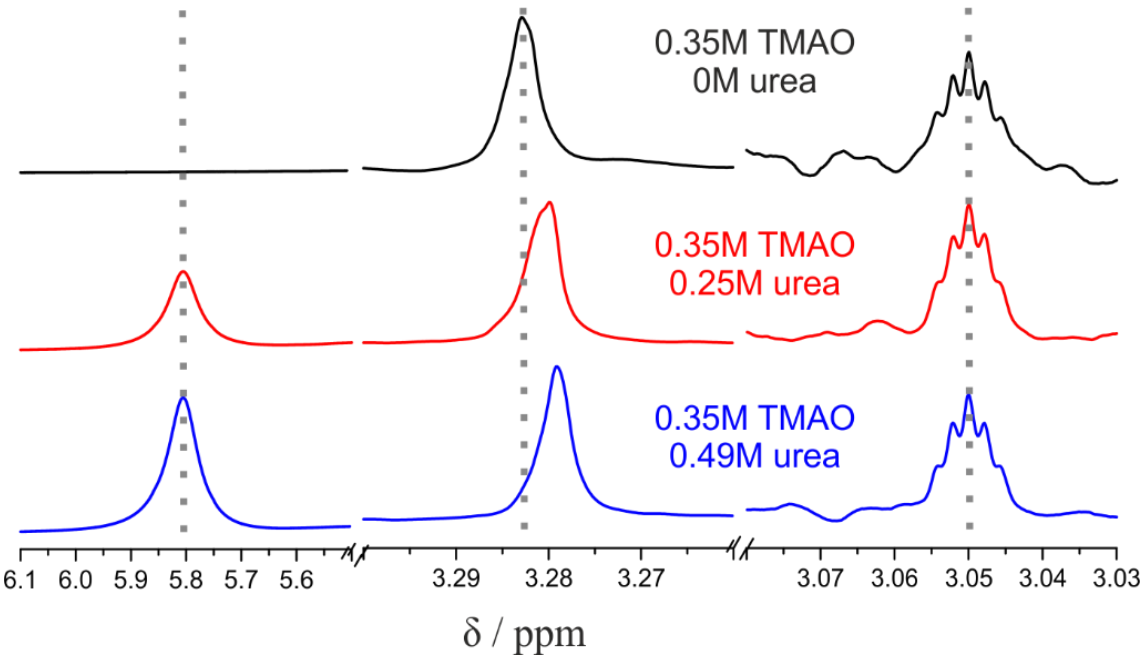

Figure S14: Representative ^{1}H NMR spectra for solutions with a constant concentration of TMAO and varying concentration of C13-urea. The signal at ~3.28 ppm due to the CH_3 groups of TMAO shifts up-field with increasing urea concentration, while the signal due to residual DMSO-d_5H at ~3.05 ppm, which was used as reference, remains unchanged. The signal at ~5.8 ppm is due to NH_2 groups of urea.

4. Supplemental Data of Computed NMR Chemical Shift

a. NMR chemical shift calculation details

We computed ^{1}H NMR chemical shifts of TMAO for the aqueous TMAO and TMAO-urea solution by using *ab initio* calculations. For this computation, took a TMAO molecule and water molecules surrounding the TMAO molecule from the AIMD (BLYP) trajectories. The water molecules were included in the chemical shift calculations, when an atom of water is within 3 Å from any atoms of TMAO. We used 100 AIMD snapshots of TMAO in water and TMAO-urea in water with the fixed distances of r = 3.85 and 5.60 Å. By averaging the computed chemical shifts over these 100 snapshots, we obtained the values of the chemical shifts for TMAO in water, TMAO with the O_{TMAO}…H_{UREA} H-bond (r = 3.85 Å), and TMAO with the hydrophobic association with urea (r = 5.60 Å).

NMR magnetic shielding tensors were computed at B3LYP, PBE0, and mPW1LYP/def2-TZVPP level of theory using gauge independent atomic orbitals (GIAO). Furthermore, to examine whether the water molecules beyond the 3.0 Å spheres around TMAO

affects the NMR shift, we considered a larger system, which included the water molecules within 5.0 Å from TMAO. This calculation was done with the ONIOM technique[S11], where the lower-level NMR calculations for the large system was done at the B3LYP/6-31G** level of theory.

The NMR chemical shift δ is given by the difference in magnetic shielding constants from a reference σ_{ref}:

$$\delta = (\sigma_{\mathrm{ref}} - \sigma)/f \qquad \text{(Equation S2)}$$

where f denotes a scaling factor. In this study, we set f and σ_{ref} to 1.1 and 31.713 ppm, respectively. σ_{ref} of 31.713 ppm was obtained from the computed ^{1}H magnetic shielding constant of TMS at B3LYP/def2-TZVPP. For all the NMR calculations, we used the polarizable continuum model to account for water beyond the explicitly treated solvation shells. We employed Gaussian 16 program suits revision A.[S12]

Our ^{1}H chemical shift calculations for TMAO in both explicit water and implicit solvent model show that the chemical shifts of nine H atoms of TMAO are not similar. Since TMAO has a C_{3v} point group symmetry, the nine H atoms can be classified into two categories; one consists of the six H atoms closer to the O_{TMAO} atom (pointed by arrows in Figure S15(a)), while the other consists of the rest of three H atoms. These sub-ensembles of the H atoms provide largely different chemical shifts (The differences are 0.33 ppm in the implicit solvent model calculation and 0.35 ± 0.04 ppm in the explicit water calculation). For the chemical shifts calculation of TMAO in water and TMAO-urea in water with *r* = 3.85 Å, we calculated the shifts by averaging individual chemical shifts over these six H atoms.

For the chemical shift of TMAO-urea in water with *r* = 5.60 Å, we focused on the two H atoms that are close to urea. Gas-phase *ab initio* calculation of a hydrophobically associates TMAO-urea system with suggested that urea affects the NMR chemical shifts of one or at most two H atoms of TMAO and the influence of urea on the other H atoms of TMAO is quite limited. Thus, we selected two H atoms among the six H atoms near the O_{TMAO} atom and averaged the chemical shifts for these two H atoms. For choosing these two H atoms next to urea, we used the criteria of the intermolecular distance of C_{UREA}…H_{TMAO} being less than 4.8 Å and the angle of C_{UREA}…H_{TMAO}-C_{TMAO} being larger than 90^{0}. A typical conformation of the TMAO-urea with *r* = 5.6 Å are depicted in Figure S15(b), together with the chosen two H atoms neighboured to urea (point by the arrows).

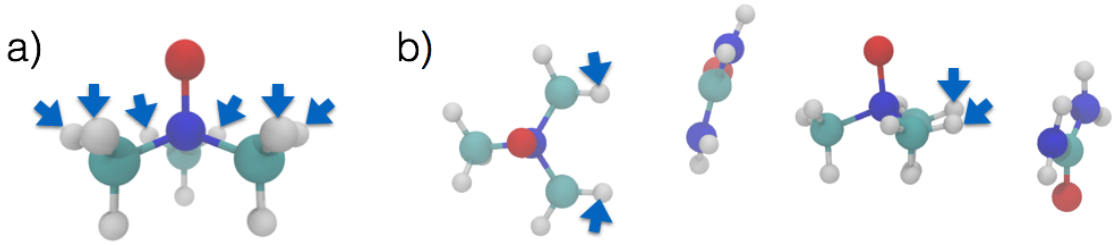

Figure S15. H atoms targeted in NMR chemical shift calculation. (a) Schematics of TMAO molecule. The arrows point the six H atoms which are close to the O_{TMAO} atom. (b) Schematics of TMAO-urea conformation at r = 5.60 Å. The arrows point at the two H atoms near urea amongst these six H atoms.

b. NMR chemical shift calculation results

The computed chemical shifts at the ONIOM theory are summarized in Table S5. The average NMR ^{1}H chemical shifts of TMAO increases upon H-bond formation between urea and TMAO (r = 3.85 Å), while it decreases when urea associates hydrophobically to TMAO (r = 5.60 Å). These trends can be seen for B3LYP, PBE0, and mPW1LYP functionals. Furthermore, we obtained the same trend, even when we did not use the ONIOM calculation.

The experimental NMR data shows the up-field shifts for ^{1}H upon the addition of urea into the aqueous TMAO solution. This is consistent with the scenario that TMAO and urea is hydrophobically associated, whereas this is at odds with the scenario that TMAO and urea can form the direct H-bonds. Thus, the experimentally measured up-field shift indicates that TMAO-urea interactions are governed by the hydrophobic interaction.

Table S5. Computed NMR proton chemical shifts of TMAO using the ONIOM-NMR technique. The unit of chemical shifts is ppm. Parenthesis values indicate standard errors.

	B3LYP	PBE0	mPW1LYP
TMAO w/o urea	3.58 (0.03)	3.69 (0.03)	3.55 (0.03)
TMAO w/ urea at r =3.85 Å	3.80 (0.03)	3.91 (0.04)	3.77 (0.03)
TMAO near urea at r = 5.60 Å	3.45 (0.04)	3.57 (0.04)	3.42 (0.04)

5. Supplemental Simulation Details

a. Force field parameters for the analyses in Figure 2 in the main text

For the analyses in Figure 2A in the main text, we varied charges of hydrophilic part of TMAO, in a manner that the partial charges of TMAO gradually changes from the Kast model to the Netz model.[39] Note that the Netz model is known to reproduce the H-bond dynamics of water.[32] We summarized the partial charges for TMAO models in Table S6. For the analyses in Figure 2B in the main text, we varied charges of urea by scaling the partial charges of the OPLS urea model[50] with different factors. We summarized the partial charges in the urea models in Table S7.

Table S6. The partial charges for TMAO models used for Figure 2A in the main text

Combination of charges	O_{TMAO} charge (*e*)	N_{TMAO} charge (*e*)
q_{Kast}[41]	-0.650	0.440
$0.75q_{Kast} + 0.25q_{Netz}$	-0.715	0.505
$0.50q_{Kast} + 0.50q_{Netz}$	-0.780	0.570
$0.25q_{Kast} + 0.75q_{Netz}$	-0.845	0.635
q_{Netz}[39]	-0.910	0.700

Table S7. The partial charges for urea models used for Figure 2B in the main text

Scaling OPLS Charge	C_{UREA} charge (*e*)	O_{UREA} charge (*e*)	N_{UREA} charge (*e*)	H_{UREA} charge (*e*)
$0.50q_{OPLS}$	0.0710	-0.195	-0.271	0.1665
$0.75q_{OPLS}$	0.1065	-0.2925	-0.4065	0.24975
q_{OPLS}[50]	0.142	-0.390	-0.542	0.333

b. TMAO-urea-water system

We performed AIMD (BLYP and revPBE) and FFMD simulations of the TMAO-urea-water mixture for computing the TMAO-urea PMF. For AIMD simulations, the simulation cell of TMAO-urea-water mixture with its size of (17.075 Å)^3 contained one deuterated TMAO (d-TMAO) molecule, one deuterated urea (d-urea) molecule and 159 D_2O molecules, resulting in a density of 1.112 g/cm^3. This corresponds to 1.001 g/cm^3 for the system with all hydrogen atoms. The system temperature was set to 380 K (for details on the effect of temperature see Section 1-b below). For computing the PMF, we constrained the distance between O_{TMAO} and C_{UREA}

ranging from 3.60 to 6.60 Å with an interval of 0.25 Å. The constraint was made by using the SHAKE algorithm.[49] The time series of the constraint forces were used for computing the PMF profile using Equation 1. With this constraint, we ran the NVT simulations.

For the FFMD simulation, we performed 8 ns FFMD runs after 1 ns equilibration in the canonical ensemble. We computed the average force for every 1 ns simulation data at each TMAO-urea separation.

For the AIMD simulation, the initial configuration at a separation of 5.10 Å between TMAO and urea was obtained from the equilibrated FFMD simulation. After 2 ps AIMD simulation for equilibration, we repeated the gradual elongation/shortening of the intermolecular distances and the equilibration with AIMD. We performed 8 independent AIMD simulations. For each the O_{TMAO}-C_{UREA} separation of the BLYP-D3 simulation, we obtained a 20 ps-long trajectory for analysis after 2 ps NVT runs to equilibrate the system. For the revPBE-D3 simulation, we obtained 23 ps-long trajectories for the O_{TMAO}-C_{UREA} constraint distance of 3.60 to 5.60 Å and 28 ps-long trajectories for the O_{TMAO}-C_{UREA} distance of 5.85 to 6.60 Å

c. TMAO-water system

For computing the dynamics of TMAO-water H-bonds, we performed an AIMD (BLYP) simulation of a d-TMAO-D_2O system and a FFMD simulation of a TMAO-H_2O system. The system contained one TMAO (d-TMAO) and 100 H_2O (D_2O) molecules for the FFMD (AIMD) simulation. The size of the simulation box was set to $(14.62\ Å)^3$. The target temperature in the NVT ensemble was set to 320 K.

For the FFMD simulation, we used the SPC/E model for water. We used the Kast TMAO model as well as the modified TMAO models (see Table S6). After 1 ns equilibration, we obtained 500 ps FFMD simulation data for analysis. The 643 ps AIMD trajectory was taken from Ref. 11.

d. Urea-water system

For computing the dynamics of urea-water H-bonds, we performed an AIMD (BLYP) simulation for a d-urea-D_2O system and a FFMD simulation for a urea-H_2O system. The system contained one urea (d-urea) and 100 H_2O (D_2O) molecules for the FFMD (AIMD) simulation. The size of the simulation box was set to $(14.60\ Å)^3$. The target temperature in the NVT ensemble was set to 320 K.

For the FFMD simulation, we used the SPC/E model for water. The data in Figure 3B in the main text were obtained using the OPLS urea model and the urea models listed in Table S7. After 1 ns equilibration, we obtained 500 ps FFMD trajectory for analysis. For the AIMD simulation, two different sets of initial coordinates were obtained from the FFMD simulations with the OPLS urea model and SPC/E water model. By using these initial coordinates, we performed

10 ps NVT runs to equilibrate the systems. Subsequently, we carried out over 80 ps AIMD runs. We finally obtained a total of 165 ps AIMD trajectories, which were used for computing the H-bond dynamics.

e. Neat water system

For computing the dynamics of water-water H-bonds, we performed AIMD (BLYP) simulations for D_2O and FFMD simulation for H_2O. For both simulations, the system contained 64 water molecules and the size of the simulation box was set to $(12.429\ \text{Å})^3$. The target temperature in the NVT ensemble was set to 320 K. For the FFMD simulation, the SPC/E model for water was used. After 1 ns equilibration, we obtained 500 ps FFMD trajectory for analysis. The 475 ps AIMD trajectory was taken from Ref. 11.

f. Energy decomposition analysis

To verify that the nature of TMAO-urea interactions differs at short and long $O_{TMAO}\cdots C_{UREA}$ distances, we performed DFT-based energy decomposition analysis (EDA) for different conformations of the TMAO-urea complex. A modified version[S13] of the second-generation absolutely localized molecular orbital (ALMO)-EDA[S14] was utilized to characterize the TMAO-urea interactions. This method is able to characterize the relative strength of electrostatics and dispersion interactions. Note that here the electrostatic interaction includes both permanent electrostatics and induced effects (polarization and charge transfer). The ALMO-EDA calculations were performed with the Q-Chem 5.0 software package,[S3] using the BLYP-D3 functional (the same functional as used for AIMD simulations) and the def2-TZVPPD basis set.[S8] 150 conformations of TMAO and urea were randomly sampled from the AIMD (BLYP) simulation trajectories with r = 3.85 Å and 5.s1 Å. These trajectories were obtained from the long AIMD simulation in Section 1-i. To examine the TMAO and urea interactions, we removed any water molecules from the snapshots of the TMAO-urea aqueous solution.

Supplemental References

S1. Holzl, C., Kibies, P., Imoto, S., Frach, R., Suladze, S., Winter, R., Marx, D., Horinek, D., and Kast, S. M. (2016). Design principles for high-pressure force fields: Aqueous TMAO solutions from ambient to kilobar pressures. J. Chem. Phys. *144*, 144104.

S2. Canchi, D. R., Jayasimha, P., Rau, D. C., Makhatadze, G. I., and Garcia, A. E. (2012). Molecular mechanism for the preferential exclusion of TMAO from protein surfaces. J. Phys. Chem. B *116*, 12095-12104.

S3. Shao, Y. H., Gan, Z. T., Epifanovsky, E., Gilbert, A. T. B., Wormit, M., Kussmann, J., Lange, A. W., Behn, A., Deng, J., Feng, X. T., et al. (2015). Advances in molecular quantum chemistry contained in the Q-Chem 4 program package. Mol. Phys. *113*, 184-215.

S4. Adamo, C., Scuseria, G. E., and Barone, V. (1999). Accurate excitation energies from time-dependent density functional theory: Assessing the PBE0 model. J. Chem. Phys. *111*, 2889-2899.

S5. Mardirossian, N., and Head-Gordon, M. (2015). Mapping the genome of meta-generalized gradient approximation density functionals: The search for B97M-V. J. Chem. Phys. *142*, 074111.

S6. Mardirossian, N., Ruiz Pestana, L., Womack, J. C., Skylaris, C.-K., Head-Gordon, T., and Head-Gordon, M. (2017). Use of the rVV10 nonlocal correlation functional in the B97M-V density functional: Defining B97M-rV and related functionals. J. Phys. Chem. Lett. *8*, 35-40.

S7. Mardirossian, N., and Head-Gordon, M. (2014). ωB97X-V: A 10-parameter, range-separated hybrid, generalized gradient approximation density functional with nonlocal correlation, designed by a survival-of-the-fittest strategy. Phys. Chem. Chem. Phys. *16*, 9904-9924.

S8. Rappoport, D., and Furche, F. (2010). Property-optimized gaussian basis sets for molecular response calculations. J. Chem. Phys. *133*, 134105.

S9. Barone, V., and Cossi, M. (1998). Quantum calculation of molecular energies and energy gradients in solution by a conductor solvent model. J. Phys. Chem. A *102*, 1995-2001.

S10. Kuo, I. F. W., and Mundy, C. J. (2004). An *ab initio* molecular dynamics study of the aqueous liquid-vapor interface. Science *303*, 658-660.

S11. Karadakov, P. B., and Morokuma, K. (2000). ONIOM as an efficient tool for calculating NMR chemical shielding constants in large molecules. Chem. Phys. Lett. 317, 589-596.

S12. Gaussian 16, R. A., Frisch, M. J., Trucks, G. W., Schlegel, H. B., Scuseria, G. E., Robb, M. A., Cheeseman, J. R., Scalmani, G., Barone, V., Petersson, G. A., Nakatsuji, H., et al. Gaussian, Inc., Wallingford CT, 2016.

S13. Mao, Y. Z., Demerdash, O., Head-Gordon, M., and Head-Gordon, T. (2016). Assessing ion-water interactions in the amoeba force field using energy decomposition analysis of electronic structure calculations. J. Chem. Theory Comput. *12*, 5422-5437.

S14. Horn, P. R., Mao, Y. Z., and Head-Gordon, M. (2016). Probing non-covalent interactions with a second generation energy decomposition analysis using absolutely localized molecular orbitals. Phys. Chem. Chem. Phys. *18*, 23067-23079.